Longitudinal dispersion in spiral wound RO modules and its effect on the performance of batch mode RO operations

T. Y. Qiu and P. A. Davies*, Sustainable Environment Research Group, School of Engineering and Applied Science, Aston University, Birmingham B4 7ET, UK

* Corresponding author: E-mail: p.a.davies@aston.ac.uk,

Tel +44 (0)121 204 3724, Fax +44 (0)121 204 3683

Abstract

Operation of reverse osmosis (RO) in cyclic batch mode can in principle provide both high energy efficiency and high recovery. However, one factor that causes the performance to be less than ideal is longitudinal dispersion in the RO module. At the end of the batch pressurisation phase it is necessary to purge and then refill the module. During the purge and refill phases, dispersion causes undesirable mixing of concentrated brine with less concentrated feed water, therefore increasing the salt concentration and energy usage in the subsequent pressurisation phase of the cycle. In this study, we quantify the significance of dispersion through theory and experiment. We provide an analysis that relates the energy efficiency of the batch operation to the amount of dispersion. With the help of a model based on the analysis by Taylor, dispersion is quantified according to flow rate. The model is confirmed by experiments with two types of proprietary spiral wound RO modules, using sodium chloride (NaCl) solutions of concentration 1000 to 20,000 ppm. In practice the typical energy usage increases by 4 to 5.5% compared to the ideal case of zero dispersion.

Keywords: Reverse osmosis; Brackish water; Dispersion; Desalination; Batch mode; Spiral wound

Symbol	Units	Description
a	m	half height (or radius) of the channel
A	m^2	cross section area of channel
C	kg m^{-3}	concentration of dissolved salt
C_f	kg m^{-3}	concentration in feed water
C_{max}	kg m^{-3}	concentration at the end of the pressurisation stage
D	m^2 s^{-1}	diffusion coefficient
k	m^2 s^{-1}	dispersion coefficient
k_h	m^2 s^{-1}	heterogeneous path dispersion coefficient
k_{Taylor}	m^2 s^{-1}	Taylor dispersion coefficient
L	m	length of the channel
L_h	m	heterogeneous path length
m_{out}	kg	mass of salt eluted during purging phase
m_r	kg	mass of residual salt
Pe		Péclet number
Q	m^3 s^{-1} (ml s^{-1})	flow rate
r		recovery ratio
r_η		efficiency ratio
t	s	time
t_{res}	s	mean residence time
$\bar{u}$	m s^{-1}	mean velocity
u_0	m s^{-1}	peak velocity
V	m^3	volume of purging water at time t
V_0	m^3	volume of the RO module
V_{max}	m^3	maximum volume of the batch-RO system
V_p	m^3	volume of purging water at cut-off point
x	m	axial position
α		retained salt ratio
β		purge cut-off point
γ		correction coefficient
σ		constant to convert the concentration to the osmotic pressure

Abbreviations

ERD	energy recovery device
RO	reverse osmosis
SEC	specific energy consumption

1. Introduction

The water crisis has become a worldwide concern and is particularly severe in remote and arid areas far from coastlines. Brackish water reverse osmosis (BWRO) has emerged as an important desalination process to provide clean water for drinking and irrigation in such areas. Owing to the competitive energy consumption of RO, the implementation of state-of-art RO systems in usually costs far less than fresh water transport by truck or pipeline [1, 2]. With appropriate implementation, these systems may make good use of the brackish water resources available. However, the U.S. Geological Survey [3] reported that only 1% of Earth's water is brackish, mainly located in estuaries as surface water and in aquifers as groundwater. Population growth and increasing water scarcity aggravated by climate change mean that brackish water resources are becoming more and more precious.

For inland BWRO desalination, one of the major challenges is brine disposal. Typical recovery ratios of BWRO systems vary from 50 to 70%, mainly depending on feed water concentration, system configuration and scale. The remaining 30 to 50% is discarded as brine. Khan et. al [4] have given a comprehensive review about brine management in which several methods of brine disposal are described and compared: surface, land application, deep well injection and evaporation ponds, etc. However, all these methods raise technical and economical concerns and, more importantly, cause significant environmental impacts [4, 5]. To minimise the brine volume and to maximise the amount of freshwater obtained, BWRO desalination systems should be designed to give a high recovery ratio.

High recovery ratio usually requires, however, large energy inputs. To overcome this drawback, a batch mode RO process that combines high recovery ratio with low specific energy consumption (SEC) has been proposed [6]. The batch system can be contrasted with the conventional continuous flow RO operation in which concentration increases significantly from the inlet to the outlet of the RO module. This longitudinal concentration gradient increases the energy requirement especially at high recovery ratios. One possible approach to minimize this effect is to provide several RO stages in series, with intermediate pumps in place to supply appropriate pressure to each stage [7, 8]. For example, a system comprising 2 stages and an energy recovery device (ERD) can in principle achieve an energy efficiency of 50% the ideal value while working at a recovery ratio of 0.7. With an infinite number of stages, the energy usage would approach the theoretical minimum. In practice this is not feasible and there will always remain some losses associated with the longitudinal concentration increase. In the batch-RO process, however, concentration is kept almost uniform through the system at each moment in time and wastage of energy due to concentration gradients inside the system is therefore minimised [6]. In principle the SEC of the batch system can approach the ideal value.

Moreover, the batch system is of particular interest for direct coupling with the solar powered Rankine cycle. To date, though several design studies [9-11] have indicated that the performance of such Rankine-RO systems should be comparable with those of photovoltaic-RO systems, practical experience has shown rather lower efficiencies [12, 13]. The batch system is expected to give significant improvements, but one factor that could compromise its performance is the longitudinal dispersion in the RO module. So, the objectives of this study are to: (i) develop a theory to represent dispersion in spiral wound RO modules and its effect on batch-RO operations; (ii) verify the theory and characterise

through experiments the dispersion in specific spiral wound RO modules typically used for brackish water desalination; (iii) as a consequence, quantify the increase in SEC that longitudinal dispersion will cause in practice.

2. Theory

2.1 The batch-RO process

The schematic of Fig. 1 illustrates the essential parts of the batch-RO system, namely a pump (having a cylinder and piston), a RO module (consisting of a membrane element housed inside a pressure vessel), a re-circulation pump and 3 valves. Each cycle of the process consists of three major phases which are listed below, while Fig. 2 shows how the concentrations at the inlet and outlet of the RO module evolve during these phases.

(1) **Pressurisation phase**, with valve 3 open while valve 1 and valve 2 are closed:
The whole system is already filled with saline water at the beginning of the cycle. The pump piston pressurises the water, causing it to pass through the membrane. The amount of solute is kept approximately constant while permeate is removed from the system. In this phase, the concentration of solution increases gradually. The concentrations at the inlet and the outlet of the module are kept nearly equal with the help of the re-circulation pump.

(2) **Purging phase**, with valve 1 and valve 2 open while valve 3 is closed:
After the pump piston reaches the end of the cylinder, only high concentration brine is left in the RO module. Therefore, it is necessary to purge the RO module by introducing feed water to wash out the brine. The concentration at the outlet decreases towards the value at the inlet.

(3) **Refill phase**, with valve 1 and valve 3 open while valve 2 is closed:
After the purging phase, the feed pump feeds saline water into the cylinder to move the piston upwards. The concentration at the outlet of the RO module decreases further, nearly reaching that at the inlet. Thus, with the whole system restored to its original conditions, the cycle is ready to start again.

Ideally, during the purging phase, the concentration of the solution at the outlet of the RO module should suddenly drop to the same value as at the input. However, dispersion causes undesirable mixing of the concentrated brine left in the RO module with less concentrated feed water, therefore increasing the salt concentration and energy usage in the following pressurisation cycle. An excess of purging water could be applied to bring down the outlet concentration, but this would waste feed water and decrease the recovery ratio of the whole operation. In order to maintain a continuous operation and achieve high recovery and efficiency, the relationship between the recovery ratio, energy consumption and dispersion needs to be established and analysed so that the operation process of the batch-RO system can be optimised.

2.2 Energy consumption vs. dispersion

The analysis assumes that the RO membrane has 100% salt rejection and that, after start up, the system runs steadily, passing through the same conditions from one cycle to the next. It is also assumed that the recirculation flow is sufficient for concentration polarisation effects

to become negligible. The recovery ratio r of the system is given as the ratio of the desalinated water produced (during the pressurisation phase) divided by the feed water supplied (during the purging and refill phases):

$$r = \frac{V_{max} - V_0}{(V_{max} - V_0) + V_p} \tag{1}$$

where V_{max} is the total maximum volume (m^3) of the system, V_0 is the minimum volume (m^3) of the system, i.e. the volume of the brine left in RO module, V_p is the volume (m^3) of the purging water used by the time at which purging is cut off. For convenience we define $V_p = \beta V_0$ and call β the purge cut-off point.

We also define the fraction of retained salt as $\alpha = m_r/m_{out}$, where m_{out} is the mass (kg) of eluted salt during the purging phase and m_r is the residual salt left in the RO module (see Fig. 4). As each cycle is assumed identical, and practically no salt passes through the membrane, the net salt eluted during the purge phase is equal to the amount supplied during the refill phase, thus:

$$C_{max} = \left[\frac{r}{(1-r)(1-\alpha)} + 1\right] C_f \tag{2}$$

where C_f is the concentration of feed water (kg m^{-3}) and C_{max} is the concentration at the end of the pressurisation stage (kg m^{-3}).

Then, the SEC for each cycle can be expressed as:

$$SEC = \frac{work\ needed\ per\ cycle}{product\ volume\ per\ cycle} = \frac{\sigma C_{max} V_p \ln(V_{max}/V_0)}{V_{max} - V_0} \tag{3}$$

where σ is the constant for converting the concentration of solution to its corresponding osmotic pressure.

Substituting Eq. (2) into Eq. (3) and simplifying gives:

$$SEC = \sigma C_f \left[\frac{1}{1-\alpha} + \frac{1-r}{r}\right] \frac{1}{\beta} \ln\left[\frac{1+(\beta-1)r}{1-r}\right] \tag{4}$$

This compares to the ideal minimum energy consumption of:

$$SEC_{ideal} = \sigma C_f \frac{1}{r} \ln\left(\frac{1}{1-r}\right) \tag{5}$$

Further details of the deductions of the above are provided in Appendix A. To achieve a high recovery and low SEC, the optimum cut-off point β should be applied. Eq. (4) can be used to determine this optimum, but first the relationship between α and β needs to be established. This requires an understanding of the dispersion phenomenon.

2.3 Dispersion in spiral wound RO modules

The analysis of dispersion in a channel depends on the geometry of the channel. Unfortunately, spiral wound membrane elements enclose a feed channel of complex geometry which is not amenable to simple analysis. A useful model, however, is that of Taylor for laminar flow through a cylindrical tube [14]. Dispersion in the spiral wound module can be expected to show similar though not identical behaviour to that in the tube. A better approximation should result from adaption of Taylor's analysis for the tube to the case of a flat channel. Even compared to the flat channel, however, the spiral wound geometry differs significantly, due to the presence of the spacer which maintains a certain height between the membranes on their feed side. Here we will apply Taylor's approach to the flat channel and incorporate adjustments to the model based on experimental observations with spiral wound modules. Note that, due to the close spacing of the membranes ($<$1mm), only laminar flow occurs in practical situations, and so the case of turbulent flow need not be considered.

Both diffusion and convection contribute to dispersion in flow through a channel. At slow flows diffusion dominates whereas at fast flow convection takes over. For flow through a tube, Probstein [15] maps the different regimes of dispersion against Péclet number $\mathrm{Pe} = \bar{u}a/D$ (where $\bar{u}$ is the mean velocity [m s^{-1}], a is the radius or half height of the channel [m] and D is the diffusion coefficient of the salt [m^2 s^{-1}]) and the tube aspect ratio (L/a, where L is the length of the channel [m]). In the range of approximately $1 < \mathrm{Pe} < L/a$, the map suggests that the dispersion coefficient may be predicted according to Taylor's expression:

$$k_{Taylor} = \frac{a^2 {u_0}^2}{192D} \tag{6}$$

In the Appendix B a similar expression is derived for a flat channel and this is applied here to the spiral wound module:

$$k_{Taylor} = \gamma \frac{8}{945} \frac{a^2 {u_0}^2}{D} \tag{7}$$

Where u_0 is the peak velocity at the centre of the channel (m s^{-1}), which is equal to 1.5 times the mean velocity $\bar{u}$. The dimensionless correction coefficient γ is included to allow for the approximations in representing the spiral feed channel as a flat channel.

Eq. (7) applies to a flat channel of uniform height with the fluid distributed perfectly evenly at its inlet. In practice, there will be non-uniformities due to manufacturing tolerances and some uneven distribution according to the detail design of the inlet and outlet manifolds. An element of fluid entering the module may therefore take a shorter or longer path through the module, resulting in a residence time distribution that is essentially independent of flow rate since this is purely a convective and not a diffusive effect. This heterogeneous path dispersion is characterised by a length L_h (m) such that the corresponding dispersion coefficient is given by:

$$k_h = \frac{{L_h}^2}{t_{res}} \tag{8}$$

where t_{res} is the mean residence time (s) of the flow. Thus, the total dispersion coefficient k for the RO module is the sum of the contributions from the mentioned two dispersion mechanisms, leading to a quadratic dependence on feed flow rate Q ($m^3\ s^{-1}$):

$$k = \gamma \frac{2}{105} \frac{a^2}{DA^2} Q^2 + \frac{{L_h}^2}{V_0} Q \tag{9}$$

where A is the cross-sectional area of the channel perpendicular to the direction of flow (m^2).

Eq. (9) shows that the dispersion coefficient increases with flow rate. This will result in greater axial mixing of the fluid and a more gradual change in concentration vs. purging volume at the outlet of the RO module. For a tube (or plane channel) initially containing a solution of zero concentration to be displaced by an incoming solution of concentration C_f, Taylor's analysis led to the following formula (which he confirmed by experiment) for concentration C as a function of axial position x from the channel entrance:

$$\frac{C}{C_f} = \frac{1}{2} - \frac{1}{2}\mathrm{erf}\left[(4kt)^{-\frac{1}{2}} x_1\right] \tag{10}$$

where erf denotes the error function, t is the time from when the new fluid starts entering the channel, and $x_1 = x - \bar{u}t$, i.e. the position researched by a particle of fluid moving at the mean speed $\bar{u}$. Our experiment is slightly different to that performed by Taylor, in that we measured the concentration at a fixed position $x = L$, corresponding to the length of the RO module, at varying time t. Thus $x_1 = L - L(V/V_0)$, where $V = Qt$ is the volume of purging solution used until time t. Our experiment also differs in the sense that the initial concentration in the channel is C_{max} to be replaced (purged) by one of lower concentration C_f. Consequently, Eq. (10) is re-written to give to the normalised concentration at the RO module outlet as:

$$\frac{C - C_f}{C_{max} - C_f} = \frac{1}{2} - \frac{1}{2}\mathrm{erf}\left[(4kt)^{-\frac{1}{2}} L\left(1 - \frac{V}{V_0}\right)\right] \tag{11}$$

At high Pe numbers (Pe≥3000), the concept of a dispersion coefficient is no longer useful. Convection dominates leading to a graph of concentration vs. purging volume V at the channel outlet that is independent of flow rate. For a simple flat channel, the expression corresponding to Eq. (11) becomes:

$$\frac{C - C_f}{C_{max} - C_f} = 1 - \left[1 - \frac{2}{3(V/V_0)}\right]^{\frac{1}{2}} \tag{12}$$

for $V/V_0 \geq 2/3$, otherwise the right hand side of Eq.(12) is equal to 1. As in the case of slow flows, the experimental results are expected to vary from this theoretical prediction, again because of the difference in geometry between the spiral wound module and the plane channel on which Eq. (12) is based. The key point of interest in Eq. (12) is the absence of any term that is dependent on flow rate Q.

3 Experiments

Experimental work was carried out at different flow rates to evaluate the above theory and thus to establish the optimum cut-off point for minimum SEC with the help of Eq. (4). The system set up is illustrated in Fig. 3. It mainly consists of the following components:

1) A saline water reservoir, containing sodium chloride (NaCl) solution.
2) A fresh (feed) water reservoir, containing tap water with a total dissolved solids (TDS) of about 60 ppm.
3) A pressure vessel, containing a spiral wound RO membrane element (Dow FILMTEC™ type BW30-2540 or XLE-2540 in separate series of experiments) with an active area of 2.6 m^2 and nominal channel dimensions of height $2a = 0.71 \times 10^{-3}$ m, length $L = 1$ m and width 1.3 m, thus giving a nominal volume of $V_0 = 0.92 \times 10^{-3}$ m^3. Both the BW30-2540 and XLE-2540 elements are of polyamide thin-film composite membrane, providing a nominal permeate flow of 3.2 $m^3 d^{-1}$, and having 99.5% and 99% salt rejection respectively, according to manufacturer specifications [16].
4) A flow-through type conductivity cell (Cole-Parmer, SN-19500-58) and transmitter (Cole-Parmer, COND 500) connected to the outlet of the RO module.
5) A data-acquisition system (LabVIEW®) to record the conductivity and time.

Both water reservoirs were placed at least 1 m above the horizontal RO module, which enabled the liquid to be driven into the RO module by gravity without using a pump. To represent conditions in the purging phase, the permeate outlet of the module was closed off, and the conductivity cell was connected to the concentrate outlet. All experiments were carried out with the solution at 20±1°C. Note that under this range of temperature, the diffusivity of NaCl in water is expected to vary by only ±0.3%. The flow rate was measured with a stopwatch and a graduated cylinder. Excess fresh water was used to flush the RO module thoroughly between experiments, in order to ensure the same starting conditions each time.

The standard operation procedure followed in all the experiments was, with reference to Fig. 3: (1) record the conductivities of saline water and fresh water separately by only opening valve 3 or 4 (with valve 1 or 2 respectively closed); (2) wash the RO module with 4×10^{-3} m^3 saline water (of the concentration of interest) by only opening valve 1 (with valve 2, 3, and 4 closed); (3) after the outlet concentration reaches a steady state, feed in fresh water by only opening valve 2 (with valves 1, 3, and 4 closed).

In a series of pilot experiments, the concentration C_{max} of saline water was varied from 1000–20,000 ppm. It was found, however, that this variation in concentration had almost no effect on the graph of normalised concentration vs. purging volume. In other words, dispersion was independent of C_{max}. The main experiments were therefore carried out with a constant value of C_{max}=3000 ppm, while the flow was varied from 0.8×10^{-6} to 40×10^{-6} $m^3 s^{-1}$ (0.8–40 ml s^{-1}).

4 Results and discussion

Fig. 4 shows an example of the normalised concentration measured at the module outlet shown as a graph against volume of purging liquid discharged. For each experimental run, a curve based on Eq. (11) was fitted to the corresponding graph by adjustment of the dispersion coefficient k. The volume V_0 was also adjusted to fit the results, but only once for the whole series of experiments corresponding to each module type, as this parameter is fixed for a particular RO module.

Though Eq. (11) gave a good representation for the first part of the graph (i.e. when normalised concentration on the vertical axis$\geq$0.5), the fit was worse for the tail of the curve corresponding to lower concentrations (see Fig. 4). This may have been due to salt trapping in the membrane leading to slow release of some salt during purging. However, the tail of the curve is hardly interesting for the batch-RO operation, because the cut-off will be applied before it is reached. Therefore least-squares fitting was applied to only the first part of the curve in order to determine k. Fig. 5 shows the values of k so obtained, for each membrane type, plotted against flow Q in the range 0.8×10^{-6}–5×10^{-6} m^3 s^{-1} (0.8–5 ml s^{-1}), the corresponding Pe number range is 320–1200, which falls in the Taylor dispersion region, i.e. $1 < \mathrm{Pe} < (L/a = 2800)$. A quadratic fitting as hypothesised by Eq. (9) enables values of γ and L_h to be obtained, as shown in Table 1. The finding that the value of γ is close to 1 confirms that the treatment of the spiral feed channel as a plane channel is reasonable at these lower flow rates. Further, the values of L_h close to 0.09 m are reasonable in relation to the module lengths of L=1 m, as the characteristic variation L_h in path length should be significantly smaller than L.

Table 1 shows also the values of V_0 determined from the experiments, which differ by as much as 16% from the nominal value of $V_0 = 0.92\text{x}10^{-3}$ m^3 based on nominal channel dimensions. This difference may be attributed to manufacturing tolerances and the volumes taken up inside the RO element by feed spacers and other features.

Fig. 6 shows the concentration curves under fast flow rates ranging from 13×10^{-6}–38×10^{-6} m^3 s^{-1} (13–38 ml s^{-1}, corresponding to 3100<Pe<10000) for the BW30-2540 membrane. As Eq. (12) predicts, the concentration curves remained almost identical and demonstrated no dependence on the flow rate. Similarly, the concentration curves for the XLE-2540 membrane were independent of flow rate (results not shown). We can conclude that the relationship between α and β is fixed at fast flow rates; this relationship is shown in Fig. 7 for each membrane type. Based on this observation, Eq. (4) enables the SEC to be determined as a function of β. The SEC is best expressed as a ratio to the ideal case corresponding to zero dispersion; thus we define the efficiency ratio $r_\eta = SEC_{ideal}/SEC$. Fig. 8 shows, for each membrane type, the relation between r_η and β under fast flow Q and a range of recovery ratios. The optimum efficiency ratio is consistently achieved when $\beta = 1$.

In future studies, improved instrumentation and control of the experimental conditions may achieve more accurate characterisation of dispersion in spiral wound modules. The theory could be extended to include further mechanisms of dispersion such as salt trapping. However, it is worth noting that an error of 10% in the dispersion coefficient results in an error of only 1% in the prediction of SEC. Therefore, our future efforts will more heavily be

directed towards investigation of other factors important for the performance of the batch-RO process, such as concentration polarisation and the parasitic power requirement of the re-circulation pump.

5 Conclusion

For the purpose of calculating SEC and recovery ratio in the cyclic batch-RO operation using spiral wound RO modules, longitudinal dispersion phenomena in the RO feed channel were analysed. Various flow rates were investigated and the dispersion behaviour was found to differ between slow and fast flows. For slow flows, corresponding to $1 < \mathrm{Pe} < L/a$, a model based on the following two mechanisms was adequate: (i) Taylor dispersion, whereby the spiral feed channel is approximated as a planar channel, and dispersion depends on feed flow, channel height and molecular diffusivity of the dissolved salt; (ii) path length heterogeneity, characterised by a dispersion length equal to 9% of the length of the RO module.

For fast flows, corresponding to $\mathrm{Pe} > L/a$, dispersion is a purely convective phenomenon and the theory and experiment show that the graph of normalised outlet concentration vs. purging volume becomes independent of flow rate. This graph was established experimentally and the relationship between retained salt fraction α and purge cut-off point β was determined. We found that the optimum cut-off is when the purge volume V_p is equal to the volume V_0 of the solution inside the module i.e. when $\beta = 1$. And at this point, the retained salt is only 8% of the total slat supplied i.e. $\alpha = 0.08$. The experiments showed that $V_0 = 0.95\times10^{-3}$ and 0.77×10^{-3} m^3 for the BW30-2540 and XLE-2540 element respectively. To reduce operation time and increase productivity, the fast flow rates are likely to be preferred in practice. In this case, the use of the optimum cut-off of $\beta = 1$ will result in deterioration in energy efficiency, relative to the ideal case of zero dispersion, in the range 4 to 5.5% for recovery ratio in the range 0.5 to 0.7. This means that the batch system should achieve high recovery ratio and thus small reject brine volume with only a minor penalty in energy efficiency.

Acknowledgements

The authors acknowledge funding from the School of Engineering and Applied Science, Aston University.

Appendix A

This appendix gives the derivation of Eq. (4).

Net salt eluted during purging phase

$$m_{out} = \int_0^{V_p} (C_{out} - C_f)\, dV = (C_{max} - C_f) V_p (1 - \alpha) \quad \text{(A.1)}$$

Salt supplied during refill phase

$$m_{in} = (V_{max} - V_0) C_f \quad \text{(A.2)}$$

According to $m_{out} = m_{in}$, Eq. (2) can be achieved.

The essential work done in the pressurisation phase is:

$$W = -\int_1^2 P \; dV = -\sigma \int_1^2 C \, dV \quad \text{(A.3)}$$

where P is pressure (Pa). According to Van't Hoff Law: $C_1 V_1 = C_2 V_2$,

$$W = -\sigma V_0 C_{max} \int_1^2 \frac{1}{V} dV = -\sigma V_0 C_{max} \ln \frac{V_{max}}{V_0} \quad \text{(A.4)}$$

So, the SEC for each cycle is expressed as Eq. (3). Eq. (4) can be obtained by substituting Eq. (2) into Eq. (3) and simplifying.

Appendix B

This appendix gives the derivation of Eq. (7). Analogous to Eq. (17) in Ref [9],

$$x_1 = x - \bar{u}t = x - \frac{2}{3} u_0 t \quad \text{(A.5)}$$

Analogous to Eq. (11) in Ref [9], where z is the non-dimensional position from the channel midline,

$$\left(\frac{\partial^2 C}{\partial z^2}\right)_x = \frac{a^2}{D}\left(\frac{\partial C}{\partial t}\right) + \frac{a^2 u_0}{D}(1 - z^2)\frac{\partial C}{\partial x} \quad \text{(A.6)}$$

Changing co-ordinates from x to x_1,

$$\left(\frac{\partial C}{\partial t}\right)_x = \frac{\partial C}{\partial x_1}\left(-\frac{2}{3} u_0\right) + \left(\frac{\partial C}{\partial t}\right)_{x_1} \quad \text{(A.7)}$$

Substituting Eq. (A.7) into Eq. (A.6), and neglecting $\frac{\partial C}{\partial t}$,

$$\left(\frac{\partial^2 C}{\partial z^2}\right)_x = \frac{a^2 u_0}{D}\left(\frac{1}{3} - z^2\right)\frac{\partial C}{\partial x_1} \quad \text{(A.8)}$$

Following the solution of Ref [19],

$$C = C_{x_1} + B\left(z^2 - \frac{1}{2} z^4\right) \quad \text{(A.9)}$$

where B is a constant given by:

$$B = \frac{a^2 u_0}{6D} \frac{\partial C}{\partial x_1} \tag{A.10}$$

The rate of transfer of concentrate across the section at x_1 is:

$$\dot{m} = -2w \int_{y=0}^{y=a} (u - \bar{u})\, C\, dy = -2wa \int_0^1 u_0 \left(\frac{1}{3} - z^2\right) C\, dz \tag{A.11}$$

Where w is the width of the channel. Inserting the value of C and B from Eq. (A.9) and (A.10), Eq. (A.11) becomes after integration:

$$\dot{m} = 2wa \frac{8}{945} \frac{a^2 {u_0}^2}{D} \frac{\partial C}{\partial x_1} \tag{A.12}$$

Thus, Eq. (7) is obtained by comparing (A.12) with Fick's law.

Table legend:

Table 1: Experimentally determined parameters for two RO elements.

Figure legends:

Figure 1 Three stages of operation of a batch-RO desalination system, from reference [6]

Figure 2 Concentration changes at the inlet (dash) and outlet (solid) of the RO module during batch mode operation

Figure 3 Lay out of the experimental system

Figure 4 Concentration vs. purging volume V at the outlet of the BW30-2540 element at feed flow 20×10^{-6} $m^3 s^{-1}$: experimental (solid), fitting curve (dot) and ideal zero dispersion curve (dash dot)

Figure 5 Dispersion coefficients under slow flows: for XLE-2540 element (left), for BW30-2540 element (right)

Figure 6 Concentration vs. purging volume V under fast flows Q (BW30-2540 element)

Figure 7 Relationship between retained salt ratio α and purge cut-off point β under fast flows Q

Figure 8 Relationship between efficiency ratio r_η and purge cut-off point β under fast flows Q for (a) BW30-2540 element and (b) XLE-2540 element. Three recovery ratios (r=0.5, 0.6, and 0.7) are shown.

References:

1. Zhou, Y. and R.S.J. Tol, *Evaluating the costs of desalination and water transport.* Water Resources Research, 2005. **41**(3): p. W03003.
2. Karagiannis, I.C. and P.G. Soldatos, *Water desalination cost literature: review and assessment.* Desalination, 2008. **223**(1-3): p. 448-456.
3. Gleick, P.H., ed. *Water resources in Encyclopedia of Climate and Weather*. ed. S.H. Schneider. Vol. 2. 1996, Oxford University Press: New York. 817-823.
4. Khan, S., et al., *Management of Concentrated Waste Streams from High-Pressure Membrane Water Treatment Systems.* Critical reviews in environmental science and technology, 2009. **39**(5): p. 367-415.
5. Younos, T., *Environmental issues of desalination.* Journal of Contemporary Water Research & Education, 2005. **132**(1): p. 11-18.
6. Davies, P.A., *A solar-powered reverse osmosis system for high recovery of freshwater from saline groundwater.* Desalination, 2011. **271**: p. 72-79.
7. Qiu, T.Y. and P.A. Davies, *Solar-powered reverse osmosis: how efficient can it be?*, in *3rd Oxford Water and Membranes Research Event*2010, Desalination and Water Treatment.
8. Elimelech, M. and W.A. Phillip, *The Future of Seawater Desalination: Energy, Technology, and the Environment.* Science, 2011. **333**(6043): p. 712-717.
9. Bowman, T., et al., *Design of a small solar-powered desalination system.* Desalination, 1981. **39**: p. 71-81.
10. Nafey, A.S. and M.A. Sharaf, *Combined solar organic Rankine cycle with reverse osmosis desalination process: Energy, exergy, and cost evaluations.* Renewable Energy, 2010. **35**(11): p. 2571-2580.
11. Bruno, J., et al., *Modelling and optimisation of solar organic Rankine cycle engines for reverse osmosis desalination.* Applied Thermal Engineering, 2008. **28**(17-18): p. 2212-2226.
12. Libert, J.J. and A. Maurel, *Desalination and renewable energies-a few recent developments.* Desalination, 1981. **39**: p. 363-372.
13. Manolakos, D., et al., *On site experimental evaluation of a low-temperature solar organic Rankine cycle system for RO desalination.* Solar Energy, 2009. **83**(5): p. 646-656.
14. Taylor, G., *Dispersion of soluble matter in solvent flowing slowly through a tube.* Proceedings of the Royal Society of London. Series A, Mathematical and Physical Sciences, 1953. **219**(1137): p. 186-203.
15. Probstein, R.F., *Physicochemical hydrodynamics*, 1995, Wiley.
16. DOW FILMTEC™ (2011). *DOW FILMTEC™ membranes product datasheet*, Form No. 609-00350-0911 and 609-00349-0811. Also available at: http://www.dowwaterandprocess.com/products/ronf.htm (accessed: Nov 11).

Table 1

Table 1

Element type	L_h (m)	γ	V_0 ($\times 10^{-3}$ m^3)
BW30-2540	0.0915	1.01	0.95
XLE-2540	0.0911	0.99	0.77

Figure 1

Figure 1

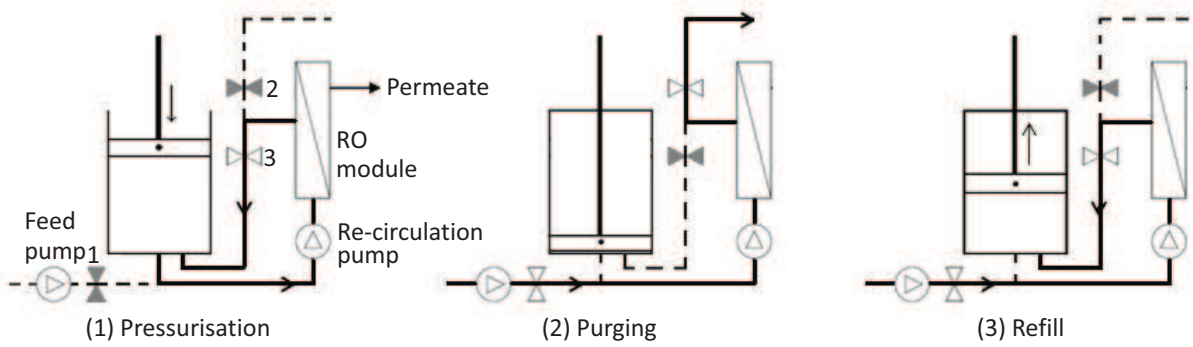

Figure2

Figure 2

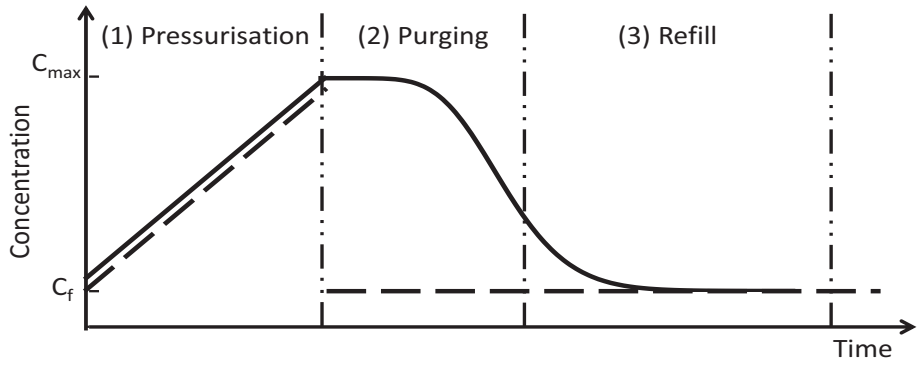

Figure3

Figure 3

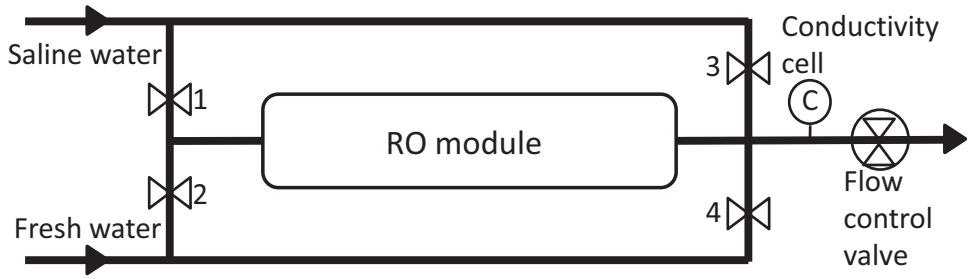

Figure4

Figure 4

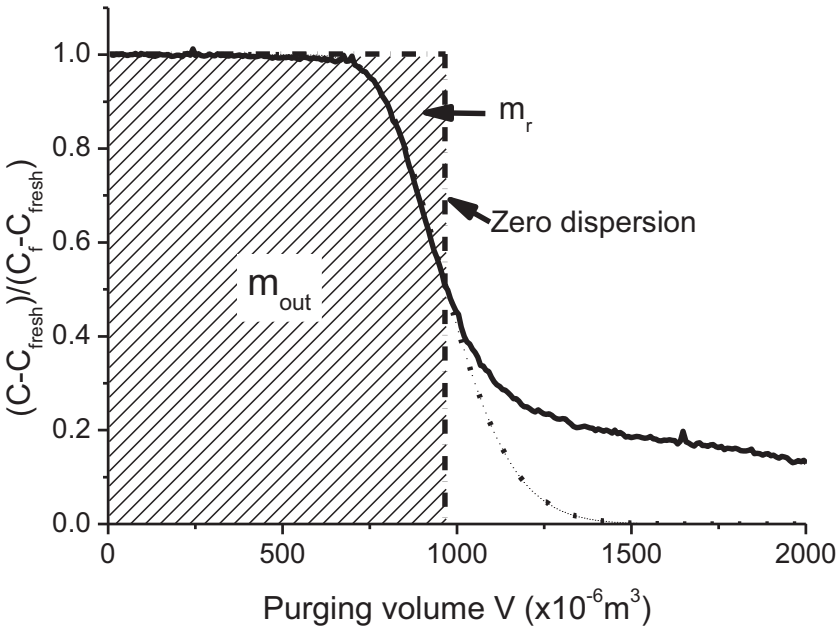

Figure5

Figure 5

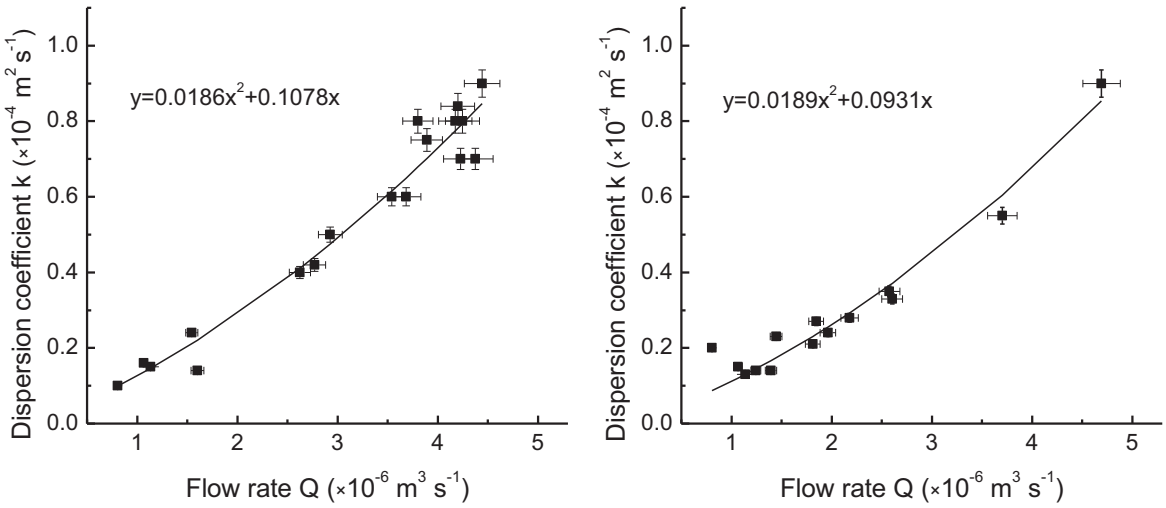

Figure6

Figure 6

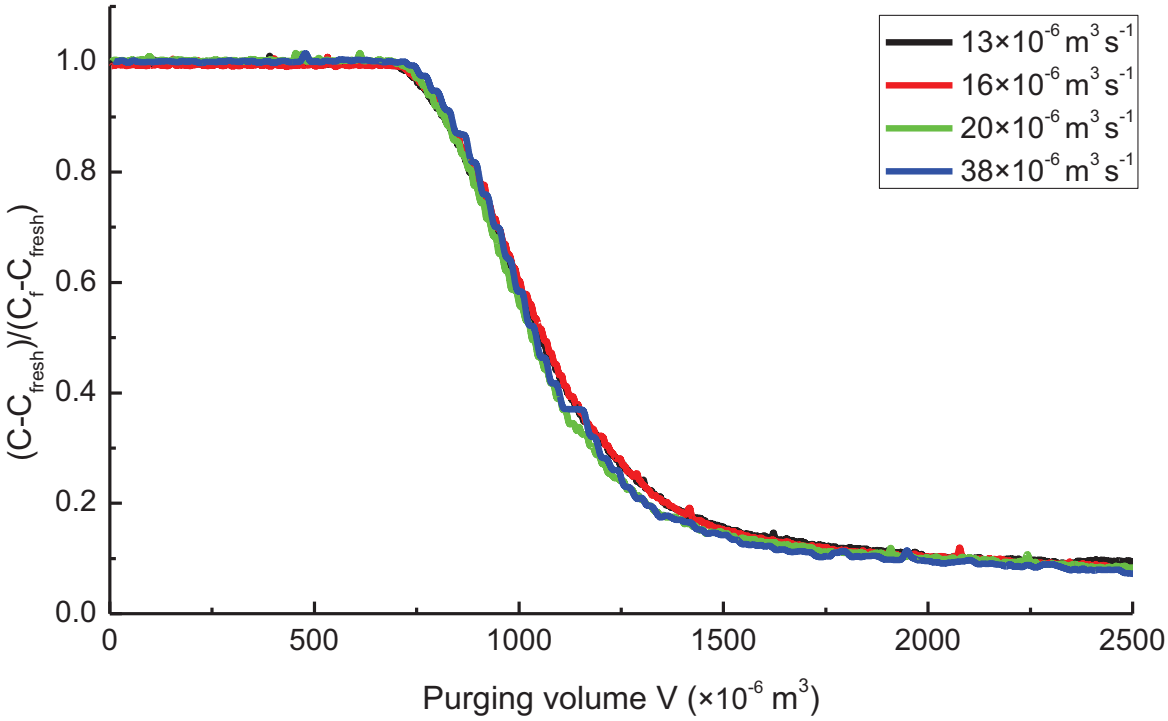

Figure 7

Figure 7

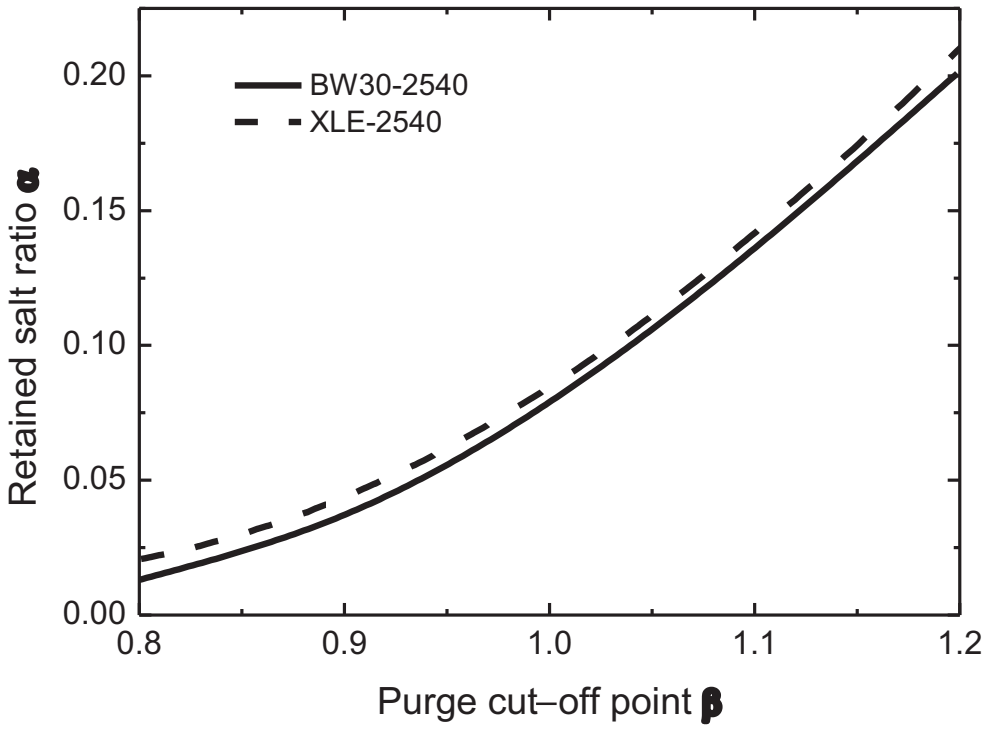

Figure 8

Figure 8